Journal of Materials Chemistry B

Accepted Manuscript

This is an *Accepted Manuscript*, which has been through the Royal Society of Chemistry peer review process and has been accepted for publication.

Accepted Manuscripts are published online shortly after acceptance, before technical editing, formatting and proof reading. Using this free service, authors can make their results available to the community, in citable form, before we publish the edited article. We will replace this *Accepted Manuscript* with the edited and formatted *Advance Article* as soon as it is available.

You can find more information about *Accepted Manuscripts* in the Information for Authors.

Please note that technical editing may introduce minor changes to the text and/or graphics, which may alter content. The journal's standard Terms & Conditions and the Ethical guidelines still apply. In no event shall the Royal Society of Chemistry be held responsible for any errors or omissions in this *Accepted Manuscript* or any consequences arising from the use of any information it contains.

ROYAL SOCIETY OF CHEMISTRY

www.rsc.org/materialsB

Journal Name RSCPublishing

ARTICLE

Cite this: DOI: 10.1039/x0xx00000x

Received 00th January 2012,
Accepted 00th January 2012

DOI: 10.1039/x0xx00000x

www.rsc.org/

Poly(ester-ether)s: III. Assessment of cell behaviour on nanofibrous scaffolds of PCL, PLLA and PDX blended with amorphous PMeDX

N. Goonoo[a], A. Bhaw-Luximon[a], I. A. Rodriguez[b], D. Wesner[c], H. Schönherr[c], G. L. Bowlin[b] and D. Jhurry[a*]

The aim of this paper is to investigate the physico-chemical properties, degradation behaviour and cellular response of electrospun fibre-scaffolds of semi-crystalline PCL, PLLA and PDX blended with amorphous poly(methyl dioxanone) (PMeDX). Electrospun PCL/PMeDX and PLLA/PMeDX blend mats in varying weight ratios of the two components were fabricated and their overall performance was compared with similar composition PDX/PMeDX scaffolds. DSC analysis showed almost no change in crystallization temperature of PCL with increasing PMeDX content and TGA showed a different degradation profile as PMeDX content increased. The appearance of two crystallization peaks for PLLA/PMeDX blends suggested stereocomplex formation. As noted from AFM images, addition of PMeDX caused a change in the width of the lamellae from 14.8 ± 2.9 nm in 100/0 mat to 32.0 ± 11.5 nm in 85/15 mat. Moreover, PCL/PMeDX blend mats show a significant drop in Young's modulus for 93/7, 90/10 and 85/15 compositions compared to 100/0 and 98/2. On the other hand, no clear trend in mechanical properties was observed for espun PLLA/PMeDX mats with increasing PMeDX content. Based on these analyses, it was concluded that PCL and PMeDX were immiscible while miscible blends were obtained with PLLA and PMeDX. Initial degradation of electrospun mats over a period of 5 weeks appears to occur via a surface erosion mechanism. *In vitro* cell culture studies using HDFs showed that the scaffolds were bioactive and a greater density of viable cells was noted on electrospun PCL/PMeDX and PLLA/PMeDX scaffolds compared to PCL and PLLA mats respectively. HDFs infiltrated through the entire thickness of espun 85/15 PLLA/PMeDX scaffold due to a combination of factors including morphology, porosity, surface characteristics and mechanical properties.

Introduction

Scaffolds for tissue engineering applications serve as a biomimetic extracellular matrix (ECM) and play a critical role in supporting cells [1]. They are designed to conform to a specific set of requirements which are often conflicting [2]. They should be biocompatible, biodegradable, porous and possess appropriate mechanical properties [3]. Electrospinning remains a preferred method due to its low cost, high throughput, ease of operation and system control. It allows the fabrication of non-woven mats containing fibres ranging from tens of microns to tens of nanometers in diameter, which can mimic both the form and function of the native ECM. Because of their mechanical properties and degradation rates that closely match those of proteins in soft and hard tissues, polymers are good candidates for the development of bone and vascular scaffolds [4]. Several natural and synthetic polymers have been investigated to this end. The most commonly used synthetic polymers are the aliphatic polyesters, polycaprolactone and poly(L-lactide) due to their relatively good biocompatibility and mechanical performance. However, cell affinities towards synthetic polymers are often poor as a consequence of their hydrophobicity and lack of cell recognition sites [5-6].

Several research groups have considered blending PCL and PLLA with other synthetic or natural polymers for optimized mechanical properties, degradation and bioactivity. Several studies have investigated the use of electrospun (espun) PCL/collagen [7-12] and PCL/gelatin [13-18] for biomedical applications. Lee *et al.* [19] reported that compared to PCL, PCL/collagen scaffolds possessed enhanced biomechanical properties that could resist higher degrees of pressurized flow. Zhang *et al.* [20] found that composite PCL and gelatin scaffold had higher elongation and better flexibility compared to PCL mat. Moreover, cells could not only grow and proliferate but also migrate inside the composite scaffold. Mehdinavaz Aghdam *et al.* [21] showed that PGA increased the hydrophilicity, water uptake and mechanical properties of polycaprolactone/polyglycolic acid (PCL/PGA) nanofibrous mats.

Journal of Materials Chemistry B Accepted Manuscript

Kim *et al.* [22] reported that the addition of PEI to PCL increased the hydrophilicity of the resulting espun mats and cell attachment on the blend mats was favoured due to the cationic nature of PEI. The miscibility of the two polymers in the blend is also an important parameter. For instance, Han *et al.* [23] studied espun blends of semi-crystalline PCL and amorphous poly(tetramethylene carbonate) (PTMC) and showed that the polymers were phase-separated in the fibres. In a recent paper, Son *et al.* [24] reported on *in vitro* and *in vivo* evaluation of espun polycaprolactone/poly(methyl methacrylate) (PCL/PMMA) fibrous scaffolds for bone regeneration. Addition of PMMA improved the wettability of the scaffolds, while decreasing PCL content caused a decrease in the tensile strength of the espun blend mats. Higher proliferation of MG-63 cells was observed on the 7/3 PCL/PMMA scaffolds.

PLLA has been blended with natural polymers such as gelatin [25-26], silk [27], chitosan [28] as well as synthetic ones such as PLGA [29] and PCL [30]. Shalumon *et al*. [28] reported that espun PLLA/chitosan blend nanofibres showed enhanced degradation and better human dermal fibroblasts (HDFs) cell growth compared to pure PLLA fibres. Liu *et al*. [29] prepared PLGA/PLLA nanofibrous mats and analysed their thermal, morphological and mechanical properties. Elongation was found to decrease with increasing PLLA content. In addition, Young's modulus and tensile strength of espun blend mats of PCL/PLLA decreased with increasing PCL content [30]. Scaffolds supported human adipose-derived stem cells (hASCs) well. However, the 1/1 wt ratio PLLA/PCL demonstrated better properties and cellular responses in all assessments.

Blending not only influences physico-chemical properties of the resulting espun mats but also impacts on their bioactivity and biological performance. It is well established that surface properties of scaffolds play a key role in cell-scaffold interactions, especially during the initial stage of cell-seeding. The topography created by the nanofibres has a strong influence on the biological response of cells seeded on its surface through contact guidance [31]. In turn, cell morphology determines cell proliferation and infiltration within a scaffold [32]. Previous studies have demonstrated that cells can recognize differences in substrate stiffness such that they can tune their internal stiffness to match that of the substrate, resulting in a change in their cytoskeletal structure [33-34]. This causes fibroblasts to adopt a more spread phenotype on stiff substrates and the cell organizes the actin cytoskeleton into stress fibres [35]. On the other hand, fibroblasts do not spread well on softer substrates and have a cortical actin cytoskeleton but no stress fibres. In fact, cell size and the spreading area increase with increasing stiffness of the substrate [36-37].

Furthermore, Cui and Sinko [38] showed that highly crystalline and rigid PCL/PGA surfaces were more efficient in supporting fibroblasts growth compared to amorphous and flexible ones. Yip *et al.* [39] showed that fibroblast behaviour was governed by strain on substrates softer than 20 kPa while the latter was dependent on stress for stiffer substrates (>20 kPa). In another paper by Lo *et al.* [40], the authors concluded on fibroblasts preference for stiff substrates. They showed that fibroblasts generate more traction force and develop a broader and flatter morphology on stiff substrates than on soft ones [40]. In addition to mechanical properties, cells are very sensitive to surface chemistry, surface energy and surface roughness [41]. In fact, surface energy plays a key role in attracting specific proteins to the surface of scaffolds which, would in turn, affect cell affinity towards these materials. Surface roughness was also found to promote cell attachment and growth on PLLA scaffolds [41]. Moreover, good hydrophobic-hydrophilic balance is crucial for optimized biocompatibility and cellular response [42]. Indeed, recent studies have shown that cells adhere, spread and grow more easily on moderately hydrophilic substrates than on hydrophobic or very hydrophilic ones [43].

In a recent study, we reported on blend films of semi-crystalline PDX and amorphous polyDL-3-methyl-1,4-dioxan-2-one (PMeDX) and showed that low amounts of PMeDX in the blends (of the order of 15 wt %) could act as plasticizer. Mechanical tests showed overall reduced tensile properties of the blend films. Interaction parameters from viscosity analysis and surface morphology images indicated immiscibility of the blend films over the range of compositions studied [44]. In another paper [45], the thermal, mechanical and degradation characteristics of espun PDX/PMeDX mats were discussed. AFM images of the espun fibres showed an increasing degree of morphological heterogeneity with increasing PMeDX content. Hydrolytic degradation of espun mats was found to be mainly dependent on fibre diameter. Espun PDX/PMeDX nanofibrous scaffolds demonstrated excellent biocompatibility as demonstrated by HDF adhesion and proliferation.

In this paper, we analyse the properties of espun mats of semi-crystalline PCL and PLLA blended with amorphous PMeDX. Our objectives are: to better apprehend the physico-chemical characteristics of espun PCL/PMeDX and PLLA/PMeDX mats; to compare the response of these two nanofibrous scaffolds to HDFs behaviour with PDX/PMeDX scaffolds described previously [45]; to attempt a correlation between physico-chemical properties and biological performance of scaffolds. The miscibility of the blends, the morphology of fibres, their thermal, mechanical properties and hydrolytic degradation as well as their efficacy to promote HDF cell growth and infiltration will be discussed. To the best of our knowledge, this is a first study where cell growth on PCL, PLLA and PDX scaffolds is compared under similar conditions.

Results and discussion

Physico-chemical and mechanical characterization of electrospun blend mats

Blends of semi-crystalline homopolymers (PCL and PLLA) and amorphous PMeDX in varying weight ratios (100/0, 98/2, 93/7, 90/10 and 85/15 wt %) were espun in HFIP at a concentration of 100 mg/ml. Thermal behaviour, fibre morphology and mechanical performance of espun PCL/PMeDX and PLLA/PMeDX mats were analysed to get a better insight into blend miscibility and surface characteristics. In particular, the effect of increasing PMeDX content on fibre diameter, pore size and porosity were investigated and compared with PDX/PMeDX fibres.

Analysis of thermal properties

DSC analysis: crystallinity and crystallization kinetics of electrospun mats

The melting temperature (T_m), enthalpy of melting (ΔH_m), crystallization temperature (T_c), enthalpy of crystallization (ΔH_c) of espun PCL/PMeDX and PLLA/PMeDX mats are summarized in Tables 1 and 2. The degree of crystallinity of the blends (χ_{blend}) and that of the PCL phase in the blends (χ_{PCL}) were calculated as reported previously [45]. The enthalpy of melting for 100 % crystalline PCL and PLLA were taken from the literature as 139.5 J/g [46] and 93.7 J/g [47] respectively.

Journal of Materials Chemistry B Accepted Manuscript

As can be noted from Table 1, espun PCL/PMeDX blend mats crystallize in the temperature range 31.2 to 33.9 °C depending on PMeDX content. The small difference in crystallization temperature suggests immiscibility of PCL and PMeDX homopolymers. It is known from the literature that when the glass transition temperature, T_g of the amorphous polymer in an immiscible blend is well below the T_c of the semi-crystalline polymer as in our case, the amorphous polymer doesn't affect T_c due to chain mobility at that temperature [48]. In contrast, the crystallization temperatures of espun PDX/PMeDX fibres were found to increase from 51.0 to 80.4 °C as the PMeDX content increased.

The plots of relative crystallinity against crystallization time (Figures 1A & B) show a sigmoid shape, indicative of a fast primary crystallization during the early stage and slow secondary crystallization in a later stage. Avrami constants, K and n which are related to crystallization kinetics and mechanism respectively were determined and the results summarized in Table 3. Variation in n values indicated that PMeDX interferes with PCL nucleation and crystallite formation with an overall increase in K value, as the PMeDX content increases. The increasing value of n in espun PCL/PMeDX blend mats compared to 100/0 denotes morphological change of crystallites, as will be discussed in the next section.

A shouldering of T_c is noted for all espun PLLA/PMeDX compositions in contrast to pure espun PLLA mat. This is attributed to stereocomplex formation. Indeed, the formation of stereocomplex has been reported for mixtures of PLLA and PDLLA where crystallization peaks at 110 and 130 °C were attributed to PLLA homocrystallites and PLLA/PDLLA stereocrystallites [49,50]. The likely formation of a stereocomplex between PLLA and PMeDX translates miscibility or partial miscibility of the two homopolymers. The Avrami K values show an overall increase in crystallization rate with increasing PMeDX content.

As can be noted in Table 2, the T_m of PLLA/PMeDX blend mats are very close to that of PLLA. A slight shouldering of T_m is observed for the 98/2 and 93/7 composition which could originate from the thermal history of the polymers. The presence of two distinct melting transitions at 175 °C and 166 °C have previously been reported for α- and β-forms of PLLA [51,52]. From Tables 1 and 2, it can also be noted that the enthalpy of fusion, ΔH_m of espun PCL/PMeDX and PLLA/PMeDX mats decrease with increasing content of amorphous PMeDX.

Table 1: DSC analysis of PCL/PMeDX espun mats

Blend composition (wt %)	Espun PCL/PMeDX non-woven mats					
	T_c/ °C	ΔH_c/ (J/g)	T_m/ °C	ΔH_m/ (J/g)	χ_{blend}/ (%)	χ_{PCL}/ (%)
100/0	31.2	52.9	57.9	44.9	32.2	32.2
98/2	32.1	52.8	57.3	43.1	30.9	31.5
93/7	33.0	50.9	56.7	43.3	31.0	33.3
90/10	33.3	51.0	56.3	40.8	29.2	32.5
85/15	33.9	42.4	55.9	35.0	25.1	29.5

Table 2: DSC analysis of PLLA/PMeDX espun mats

Blend composition (wt %)	Espun PLLA/PMeDX non-woven mats							
	T_{c1}/ °C	T_{c2}/ °C	ΔH_c/ (J/g)	T_{m1}/ °C	T_{m2}/ °C	ΔH_{m1}/ (J/g)	ΔH_{m2}/ (J/g)	χ_{blend}/(%)
100/0	149.6	-	56.9	178.0	-	57.6	NA	61.4
98/2	115.9	122.2	43.3	175.0	165.8	34.5	12.5	50.2
93/7	114.7	106.9	43.8	175.6	167.2	37.8	7.47	48.4
90/10	124.4	109.7	37.4	177.0	-	43.9	-	46.8
85/15	115.8	108.5	31.2	177.3	-	42.5	-	45.3

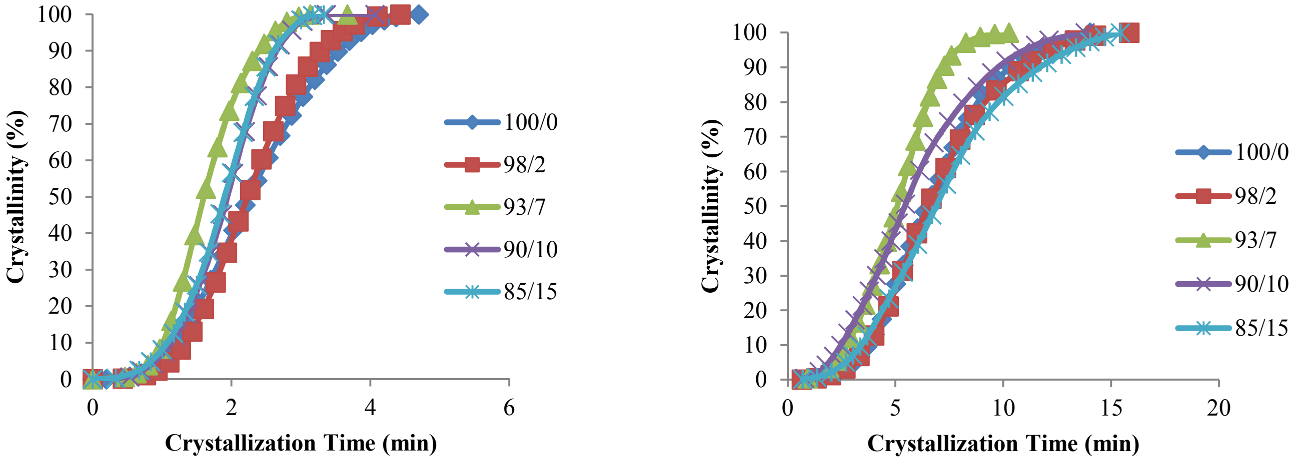

(A) (B)

Figure 1: Plots of relative crystallinity versus crystallization time for espun (A) PCL/PMeDX and (B) PLLA/PMeDX mats

Journal of Materials Chemistry B Accepted Manuscript

Table 3: Summary of Avrami parameters for espun PCL/PMeDX and PLLA/PMeDX

Espun PCL/PMeDX mats					
	100/0	**98/2**	**93/7**	**90/10**	**85/15**
K	0.29	0.24	0.37	0.31	0.36
n	2.95	3.53	3.64	3.59	3.29
Espun PLLA/PMeDX mats					
	100/0	**98/2**	**93/7**	**90/10**	**85/15**
K	0.07	0.07	0.10	0.14	0.09
n	2.93	2.96	3.12	2.41	2.58

Thermogravimetric Analysis (TGA)

Thermal degradation profiles of espun PCL/PMeDX and PLLA/PMeDX mats are shown in Figures 2 and 3 respectively. Espun PCL mat shows a two stage degradation profile with an onset degradation temperature, T_{onset} at 374.6 °C. PMeDX, on the other hand, degrades in a single step with a much lower T_{onset} of 78 °C. Espun 98/2 PCL/PMeDX follows a similar degradation profile as the 100/0 mat with no change in T_{onset} (Table 4). This suggests that PMeDX may be partially miscible at that composition. This is also confirmed by mass loss calculations whereby PCL and PCL/PMeDX 98/2 have comparable mass loss. However, with increasing PMeDX contents (7, 10 & 15 wt %), the degradation profile changes with a first-step degradation occurring at a lower temperature. Mass loss calculations ΔW_1 is equivalent to the initial wt % of PMeDX for these blend compositions (Table 5), which denotes degradation of PMeDX in the blend This supports immiscibility of PCL and PMeDX homopolymers, in line with DSC data.

Espun PLLA mat show a T_{onset} of 324.2 °C and increasing PMeDX content led to decreased thermal stability of PLLA (Table 4) with T_{onset} dropping from 324.2 to 306.5 °C. In contrast to PCL/PMeDX blend mats, only one degradation stage was noted for all espun PLLA/PMeDX mats. This further supports the formation of PLLA/PMeDX stereocomplex as proposed in the previous section.

On the basis of these results, it can be suggested that immiscibility increases with increasing PMeDX content for PCL/PMeDX, with the 98/2 blend being partially miscible. Moreover, the formation of stereocomplex between PLLA and PMeDX is confirmed by TGA.

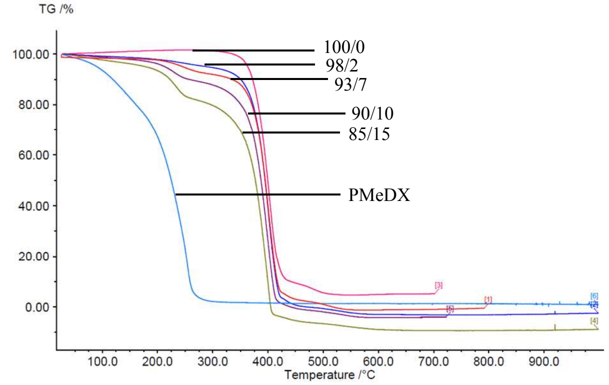

Figure 2: TGA profiles of espun PCL/PMeDX mats

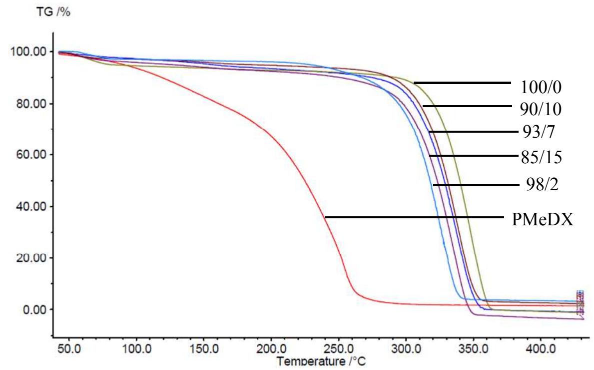

Figure 3: TGA profiles of espun PLLA/PMeDX mats

Table 4: Variation of onset degradation temperatures of espun fibres

Blend composition (wt %)	Espun PCL/PMeDX fibres			Espun PLLA/PMeDX fibres	
	T_{onset}/ °C	T'_{onset}/ °C	T_{max}/ °C	T_{onset}/ °C	T_{max}/ °C
100/0	374.6	432.0	405.3	324.2	348.9
98/2	374.3	424.0	400.0	321.1	348.8
93/7	214.3	375.7	402.2	327.2	338.8
90/10	201.4	370.2	400.8	312.4	340.2
85/15	206.6	368.8	399.3	306.5	335.8

T_{onset}: Onset degradation temperature for 100/0 and 98/2 (one stage)
T'_{onset}: Onset degradation temperature for first stage degradation of 93/7, 90/10 and 85/15

Table 5: Mass loss derived from TG degradation profiles

Blend composition (wt %)	Espun PCL/PMeDX fibres			Espun PLLA/PMeDX fibres
	ΔW_1/ (wt %)	ΔW_2/ (wt %)	ΔW_3/ (wt %)	ΔW_1/ (wt %)
100/0	-	91.7	4.09	97.9
98/2	-	96.2	5.96	98.7
93/7	6.68	92.6	-	99.1
90/10	10.3	90.8	-	97.6
85/15	15.2	85.9	-	99.9

ΔW_1: Mass loss corresponding to first decomposition stage in 93/7, 90/10 and 85/15
ΔW_2: Mass loss corresponding to major decomposition stage in all blends
ΔW_3: Mass loss corresponding to second decomposition stage in 100/0 and 98/2 blend

FTIR Analysis

FTIR spectrum of espun PCL and PMeDX homopolymer showed characteristic C-O stretching bands at 1643 cm^{-1} and 1732 cm^{-1} respectively. Espun PCL/PMeDX blends showed bands between 1743-1696 cm^{-1} and between 1631-1650 cm^{-1} depending on PMeDX content (Figure 4, Table 6). Significant shift in PMeDX carbonyl for

Journal of Materials Chemistry B Accepted Manuscript

98/2 blend composition (1696 cm^{-1}) suggests some interaction with PCL.

The stretching vibration of PLLA was found at 1631 cm^{-1}. For espun PLLA/PMeDX mats, only one band was observed contrary to PCL/PMeDX mats. A slight shift in carbonyl stretching (4 cm^{-1}) was noted with increasing PMeDX content.

In summary, FTIR analysis suggests immiscibility of espun PCL/PMeDX mats and plasticization at low PMeDX content (2 wt %) while PLLA and PMeDX appear to be miscible based on the appearance of a single band.

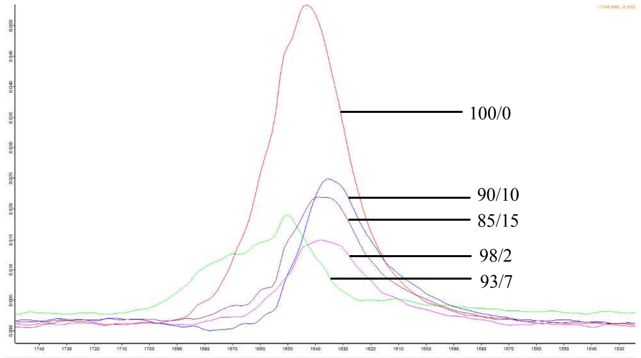

Figure 4: FTIR spectra of espun PCL/PMeDX mats

Table 6: Variation of $\nu_{(C=O)}$ in espun PCL/PMeDX and PLLA/PMeDX

Blend composition/ (wt/wt)%	$\nu_{(C=O)/}$ cm^{-1}	*Shoulder at* $\nu_{(C=O/}$ cm^{-1}
100/0	1643	-
98/2	1638	1696
93/7	1650	1743
90/10	1635	1713
85/15	1639	1714

AFM analysis

Surface Morphology

AFM images (Figures 5A & B) show that both espun PCL and PCL/PMeDX nanofibres exhibit cylindrical morphology. Espun PCL mats had a smooth surface in contrast to blend nanofibres (85/15) which showed a rougher surface, possibly due to dispersion of PMeDX within the PCL matrix. Indeed, as reported by Leclair *et al.* [53], deformations of the rubbery amorphous polymer occur in an immiscible semi-crystalline/amorphous polymer blend if the latter is above its T_g during crystallization of the semi-crystalline polymer (T_g PMeDX= 20 °C, T_c PCL= 33 °C).

More in-depth analysis of AFM images were carried out to investigate the nanostructure of the espun mats. Figure 6A shows the lamellar crystal morphology within PCL spherulites crystallized at room temperature. A clear morphological change is observed with the addition of PMeDX as shown in Figure 6B. Indeed, the presence bright domains within the lamellae can be seen in Figure 6B. The bright regions possibly correspond to amorphous phase as reported by Gomez-Pachon *et al.* [54].

Moreover, addition of PMeDX caused a change in the width of the lamellae from 14.8 ± 2.9 nm in 100/0 mat to 32.0 ± 11.5 nm in 85/15 mat, suggesting that PMeDX influences PCL crystallization as already noted from Avrami constants, K and n in the discussion on DSC analysis. This confirms that PMeDX interferes with PCL nucleation and crystallite formation.

PLLA/PMeDX fibres do not show clear structures as for PCL/PMeDX but exhibit corrugation-like patterns (Figure 7) whereas some PLLA fibres show a regular wavy pattern perpendicular to the direction of the fibres. The lamellae appeared very thin and were arranged in a parallel manner but with changing orientation relative to the fibre, unlike in the case of espun PDX fibre (Figure 8).

Fibre diameter and pore size

Table 7 summarizes fibre diameters and pore sizes as determined by SEM as well as porosity values based on calculations described in the experimental section. Overall, fibre diameters decrease with increasing PMeDX wt % for both espun PCL/PMeDX and PLLA/PMeDX fibres while no clear trend was observed for PDX/PMeDX fibres, data was more erratic due to protrusions on the fibre surface and no clear trend was observed [45]. The decrease is explained by the fact that fibre diameter of espun binary blends of incompatible polymers is dependent on the internal phase morphology and solution viscosity. Indeed, if the dispersed phase in the blend has a lower viscosity, as that of PMeDX, the solution jet will be stretched and elongated more by the electric forces during the electrospinning process [55]. However, the decrease in fibre diameter was more pronounced for PCL/PMeDX fibres compared to PLLA/PMeDX due to its higher elasticity and stretchability.

However, as for espun PDX/PMeDX fibres, there was no clear cut trend in pore size for both espun PCL/PMeDX and PLLA/PMeDX fibres. Porosity values were found to increase slightly with increasing PMeDX content in both cases which may suggest a decrease in fibre packing density.

Table 7: Effect of PMeDX wt % on fibre diameters

Blend composi tion (wt/wt) %	**Fibre Diameters/ (μm)**	**Inside Pore size/ (μm)**	**Outside Pore size/ (μm)**	**Porosity**
Espun PCL/PMeDX mats				
100/0	0.35 ± 0.26	1.2 ± 0.79	0.83 ± 0.27	12.3 ± 0.9
98/2	0.27 ± 0.15	0.78 ± 0.34	0.68 ± 0.31	14.5 ± 1.3
93/7	0.28 ± 0.21	0.63 ± 0.24	0.56 ± 0.19	20.1 ± 1.1
90/10	0.25 ± 0.13	0.58 ± 0.22	0.60 ± 0.25	23.2 ± 1.5
85/15	0.23 ± 0.10	0.62 ± 0.23	0.72 ± 0.24	27.4 ± 1.7
Espun PLLA/PMeDX mats				
100/0	0.33 ± 0.11	0.68 ± 0.34	0.73 ± 0.37	13.7 ± 0.6
98/2	0.34 ± 0.11	0.79 ± 0.43	0.89 ± 0.38	14.4 ± 1.6
93/7	0.34 ± 0.10	0.82 ± 0.33	0.57 ± 0.21	18.8 ± 1.2
90/10	0.30 ± 0.09	0.67 ± 0.24	0.81 ± 0.33	20.1 ± 1.8
85/15	0.30 ± 0.08	0.64 ± 0.26	0.71 ± 0.27	25.7 ± 2.1

In general, the extent of whipping motion determines fibre diameter. When the electrospinning jet experiences more whipping motion with crystallization most likely occurring before the jet reaches the

Journal of Materials Chemistry B Accepted Manuscript

This journal is © The Royal Society of Chemistry 2012

collector, small diameter fibres result with fibrillar structures. Large diameter fibres experience less whipping and crystallization is most likely to occur after the jet reaches the collector [56].

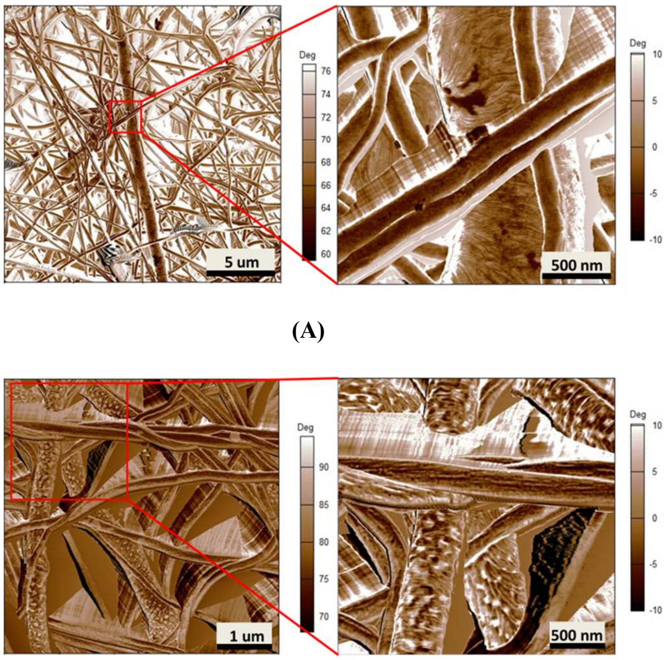

(A)

(B)

Figure 5: AFM phase images of espun PCL/PMeDX (A) 100/0 (B) 85/15 fibres

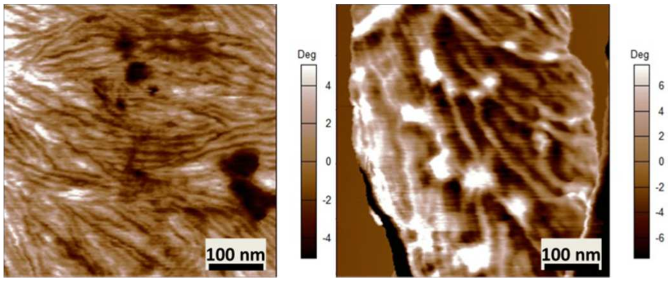

(A) (B)

Figure 6: AFM image of espun PCL (A) and espun 85/15 PCL/PMeDX mat (B) showing morphological change of crystallites

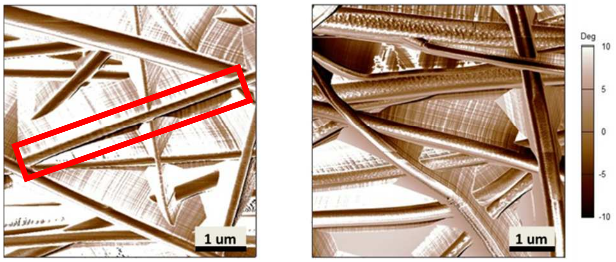

(A) (B)

Figure 7: AFM phase images of espun PLLA/PMeDX (A) 100/0 and (B) 85/15

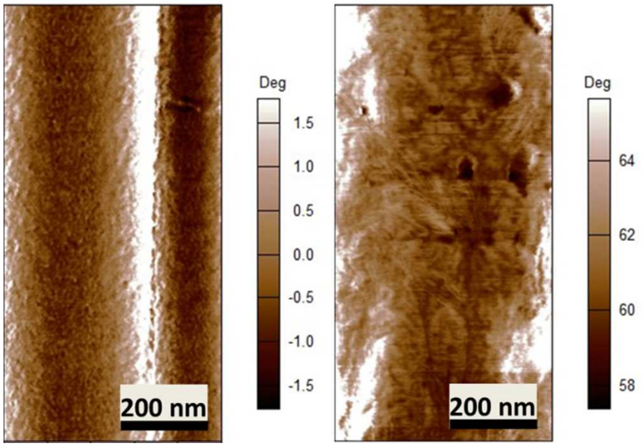

(A) (B)

Figure 8: AFM phase image of espun (A) PLLA/PMeDX (85/15) and (B) PDX fibre

Mechanical performance

Mechanical properties of espun fibres depend on a combination of several factors such as fibre alignment, fibre diameter, fibre lay-ups and interface properties of fibre-fibre contact (fibre fusion) [57,58]. Tensile properties of fibres are affected by their structural morphology. In fact, the strength and elastic modulus of fibres is influenced by the lamellar and amorphous fractions of chains present within fibres. Elastomeric property of fibres is due to the amorphous phase of the fibres while dimensional stability is attributed to the crystalline phase [59]. Thus, the mechanical deformation characteristic of the fibre is influenced by both the random amorphous and ordered crystalline phases in the fibre [59]. The internal micro/nanostructural morphology of nanofibres determines their physical and mechanical properties [60]. As reported in previous studies, changes in lamellae alignment and thickness result in variations of mechanical properties [61]. Saffar *et al.* [62] demonstrated that elongation at break decrease with crystalline orientation. Also, Bozic *et al.* [63] showed that substrates with coarse lamellar structures possessed higher elongation compared to those with fine lamellar microstructures.

As reported in our previous paper [45], the Young`s modulus of espun PDX/PMeDX mats decrease with increasing PMeDX wt %. Also, in general, both strain at break and peak stress increase with decreasing fibre diameters. PCL/PMeDX blend mats show a significant drop in Young’s modulus for 93/7, 90/10 and 85/15 compositions compared to 100/0 and 98/2 (Table 8, Figure 9). It is likely that the formation of phase boundaries impact on mechanical performance more than crystallinity changes [64].

On the other hand, the interpretation of mechanical properties for PLLA/PMeDX blends is more difficult as no clear trend is observed with increasing PMeDX content (Table 9, Figure 10). This could be due to antagonist effects such as drop in crystallinity which impacts negatively on mechanical properties (98/2 composition) and formation of stereocomplex which could enhance (93/7 and 90/10) but in other cases (85/15) limit mechanical performance. This can be explained by the stereocomplex formation based on thermal analysis data where the percentages of homoPLLA crystallites and PLLA/PMeDX stereocomplex crystallites may affect mechanical performance.

Journal of Materials Chemistry B Accepted Manuscript

Table 8: Mechanical properties of espun PCL/PMeDX mats

PCL/PMeDX composition (wt %)	Tensile strain (mm/mm)	Modulus (MPa)	Extension at break (mm)
100/0	0.14 ± 0.03	5.33 ±0.025	10.33
98/2	0.13 ± 0.007	5.19 ± 0.026	9.58
93/7	0.11 ± 0.002	3.54 ± 0.004	8.12
90/10	0.08 ± 0.002	1.41 ± 0.003	6.44
85/15	0.13 ± 0.005	2.86 ± 0.011	9.56

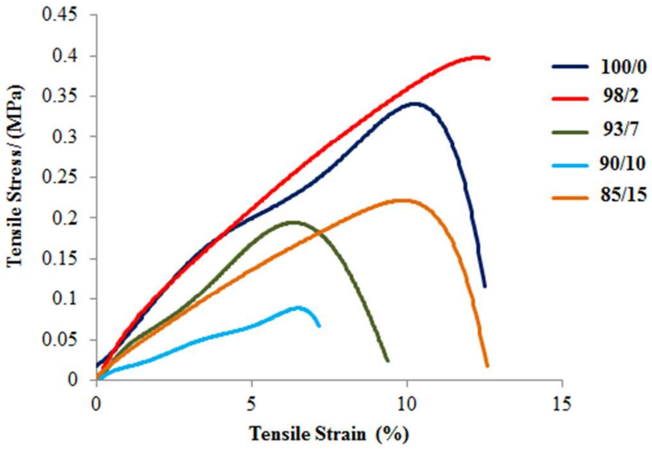

Figure 9: Stress-strain curves of espun PCL/PMeDX mats

Table 9: Mechanical properties of espun PLLA/PMeDX mats

PLLA/PMeDX composition (wt %)	Tensile strain (mm/mm)	Modulus (MPa)	Extension at break (mm)
100/0	1.40 ± 0.022	9.65 ± 0.100	14.05
98/2	1.00 ± 0.007	4.57 ± 0.031	10.01
93/7	0.89 ± 0.001	17.24 ± 0.018	8.90
90/10	1.25 ± 0.0007	30.11 ± 0.018	12.55
85/15	1.00 ± 0.003	4.78 ± 0.019	10.01

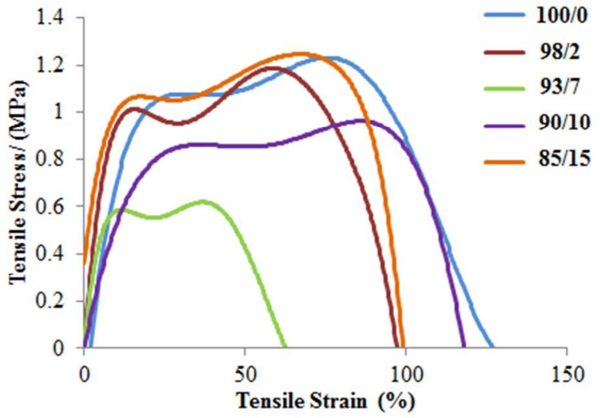

Figure 10: Stress-strain curves of espun PLLA/PMeDX mats

Hydrolytic degradation studies

Hydrolytic degradation of espun mats was carried out in PBS at 37 °C for 5 weeks. We have shown recently that degradation of espun PDX/PMeDX mats occurred via surface erosion and was found to be dependent on fibre diameter of the fibres [45]. Larger diameter espun 98/2 PDX/PMeDX mat degraded at a faster rate than smaller diameter 85/15 mat. Similarly, espun PCL/PMeDX and PLLA/PMeDX mats appear to degrade via a surface erosion mechanism during the time period investigated as noted by the slight drop in pH (Figure 11) and linear mass loss profiles (Figure 12). Mass loss profiles showed enhanced degradation with increasing PMeDX content which can possibly be explained by a combination of factors: decreased crystallinity in the blends, reduced fibre diameters and higher porosities. Mass loss profiles show that espun PCL/PMeDX and PLLA/PMeDX exhibit almost similar degradation rates. For instance, 93/7 PCL/PMeDX and PLLA/PMeDX mat had a mass loss of about 7.2 and 5.7 % at week 5 and 85/15 PCL/PMeDX and PLLA/PMeDX mat had a mass loss of approximately 9.3 and 7.5 % respectively at week 5. It has to be pointed out that mass loss values correspond to a relatively short degradation time. Zhao *et al.* [65] also observed linear mass loss profiles for the hydrolytic degradation of espun PLLA and PLLA/hydroxyapatite mats.

Degraded samples were analysed by SEM. Figure 13 depicts SEM images of espun 98/2 and 85/15 PCL/PMeDX and PLLA/PMeDX mats after 5 weeks of degradation. Both 98/2 PCL/PMeDX and PLLA/PMeDX mats show no change in morphology at week 5. However, the 85/15 PCL/PMeDX mat shows fibre melting which is not observed in the corresponding PLLA/PMeDX mat. This can possibly be explained by the smaller fibre diameter of the 85/15 espun PCL/PMeDX mat.

Journal of Materials Chemistry B Accepted Manuscript

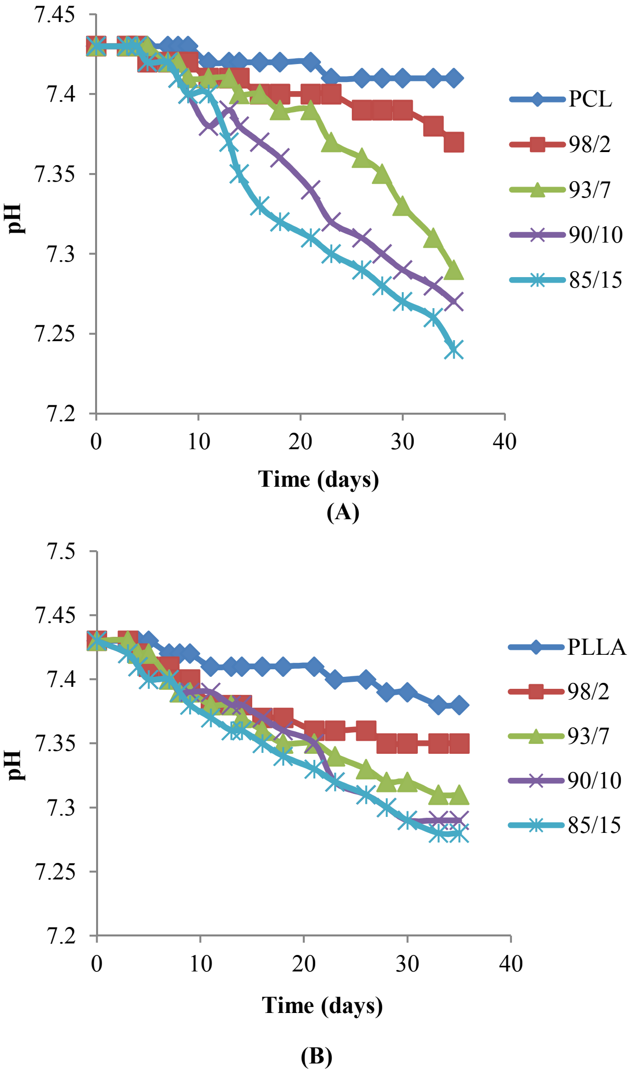

(A)

(B)

Figure 11: pH evolution of (A) PCL/PMeDX and (B) PLLA/PMeDX mats with varying PMeDX wt %

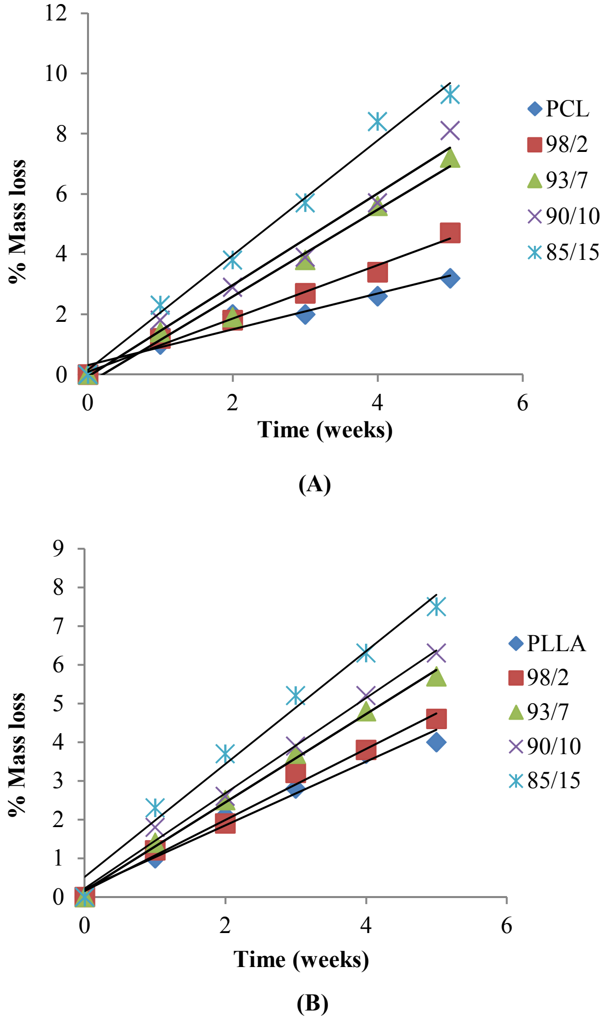

(A)

(B)

Figure 12: Mass loss of (A) PCL/PMeDX and (B) PLLA/PMeDX mats as a function of hydrolysis time in PBS at 37 °C

Journal of Materials Chemistry B Accepted Manuscript

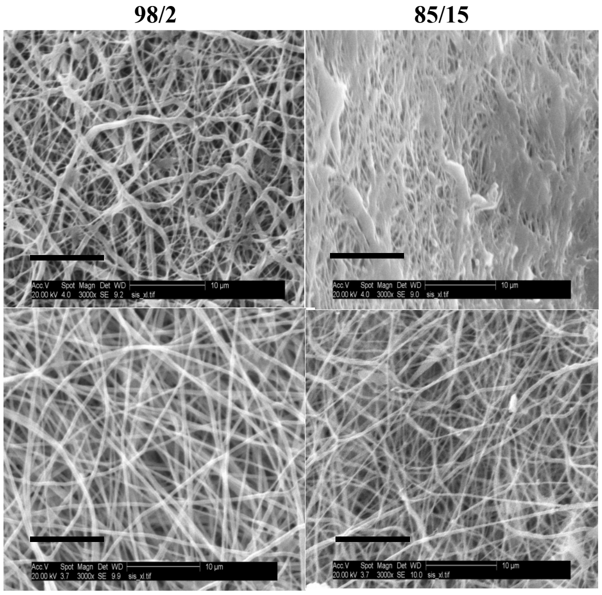

Figure 13: SEM (3000× magnification, scale bar = 10 µm) of espun 98/2 and 85/15 PCL/PMeDX (top) and PLLA/PMeDX (bottom) mats at week 5

In vitro biocompatibility studies

We have previously shown that addition of PMeDX to espun PDX fibres resulted in a greater density of viable human dermal fibroblasts compared to espun PDX mat with cells migrating up to a maximum of 45.1 ± 11.8 % throughout the scaffold after 7 days [45]. This was attributed to smaller fibre packing density and higher porosity. Espun PCL/PMeDX and PLLA/PMeDX mats were subjected to cell viability studies to investigate the effect of PMeDX incorporation in PCL and PLLA. Human dermal fibroblasts (HDFs) were cultured and seeded on the scaffolds for a period of up to 7 days.

Cell attachment and proliferation

Figures 14 and 15 show the SEM images of HDFs cultured on espun PCL/PMeDX and PLLA/PMeDX scaffolds after 1 and 7 days respectively. In general, it was observed that cells spread over the mat surface. Compared to espun PCL or PLLA mats, a higher density of cells was found on PCL/PMeDX and PLLA/PMeDX scaffolds as from day 1.

A change in cell morphology was noted with increasing PMeDX content from bipolar spindle (as red marked in Figure 14) to a cobble-stone morphology with poorly organized actin filaments (Table 10) which was more pronounced with PLLA/PMeDX than PCL/PMeDX. This suggests that higher PMeDX content results in poor cell adhesion, causing the cells to adopt a cobble-stone morphology with few filopodia as can be seen in espun 85/15 PCL/PMeDX mat (Figure 16). The cobble-stone shaped cells seem to be covered with deposited material, which is most probably ECM. Despite poor adhesion to the substrate, the balled up cells proliferated and produced matrix to create a conducive environment. As discussed in previous sections, addition of PMeDX to PLLA alters mechanical properties and crystallinity more significantly compared to PCL and as highlighted in the introduction, cell growth is influenced by changes in crystallinity and mechanical properties of the substrate. The presence of cobble-stone HDF morphology was detected as from 15 wt % PMeDX for PCL/PMeDX mat and as early as 2 wt % PMeDX for PLLA/PMeDX mat. A change in fibroblast morphology from elongated, oriented to cobble-stone was observed with the application of shear stress as reported by Braddon *et al.* [66]. The change in HDF morphology can be explained by the change in microstructures of espun fibres. Ajami-Henriquez *et al.* [67] reported that the presence of lamellae promotes "cell contact-guidance". In fact, they showed that other factors such as chemical composition, degree of crystallinity and surface roughness did not play a major role in determining cell preference towards a specific material. Based on the above, we deduce that the presence of lamellae in espun PCL/PMeDX fibres may account for the fact that cells grown on these surfaces were mostly spindle-shaped. Furthermore, cobble-stone morphology observed on espun PLLA/PMeDX mats can possibly be related to the absence of lamellae on the mats.

In contrast, no change in morphology was observed for PDX/PMeDX mat with 0-15 wt % PMeDX when subjected to cell growth. An increasing degree of heterogeneity and surface roughness noted with increasing amorphous PMeDX in espun PDX/PMeDX mats [45] could explain enhanced cell adhesion. It was therefore hypothesized that surface roughness in espun PDX/PMeDX was the dominant factor on fibroblasts proliferation compared to the decrease in crystallinity.

Cell behaviour has been reported to be dependent on three factors namely, percentage cell coverage of the surface, pore size and cell type. Indeed, as demonstrated by Salem *et al.* [68], fibroblasts displayed a co-operative pattern of cell spreading whereby pores greater than cell dimensions were bridged by group of cells using their neighbours as supports.

Table 10: Influence of crystallinity and tensile strain on cell morphology

Blend composition (wt/wt %)	Cell morphology	Crystallinity χ_{blend}/(%)	Tensile strain/ (mm/mm)
Espun PCL/PMeDX			
100/0	Bipolar spindle	32.2	0.14
98/2	Bipolar spindle	30.9	0.13
93/7	Bipolar spindle	31.0	0.11
90/10	Bipolar spindle	29.2	0.08
85/15	Cobble-stone	25.1	0.13
Espun PLLA/PMeDX			
100/0	Bipolar spindle	61.4	1.40
98/2	Cobble-stone	50.2	1.00
93/7	Cobble-stone	48.4	0.89
90/10	Cobble-stone	46.8	1.25
85/15	Cobble-stone	45.3	1.00

As depicted in Table 10, the decreasing crystallinity of the blends with increasing PMeDX wt % here implies an enhanced flexibility of the corresponding mats and in accordance with the introductory paragraph explains poorer cell adhesion especially in the case of PLLA/PMeDX mats where only 2 wt % PMeDX causes a drop of 10 % in crystallinity.

As discussed in the Introduction, previous reports have shown that fibre diameter, porosity and surface roughness influence surface hydrophobicity which also affects cell behaviour. To have a better insight into surface hydrophobicity, contact angles were measured for a few samples and are listed in Table 11. Compared to PCL, the

Journal of Materials Chemistry B Accepted Manuscript

contact angle of a 93/7 PCL/PMeDX mat is nearly halved which translates a significant increase in surface hydrophilicity. The same trend was previously noted for espun PDX/PMeDX where the contact angles decreased upon increasing content of PMeDX [45]. Interestingly, cell adhesion appeared optimal for this 93/7 PCL/PMeDX mat, with extensive ECM secretion by day 7. This supports the fact that higher hydrophilic surfaces promote cell adhesion. On the other hand, increasing PMeDX in PLLA/PMeDX mats did not cause significant change in surface contact angles. This could partly explain the poor adhesion of cells onto PLLA/PMeDX mats, as we highlighted in the previous paragraphs.

Table 11: Summary of static contact angle measurements on espun PCL/PMeDX and PLLA/PMeDX mats

Espun PCL/PMeDX	
Blend composition (wt/wt %)	**CA (Mean ± SD)**
100/0	131.6 ± 2.5
93/7	63.1 ± 2.1
Espun PLLA/PMeDX	
100/0	127.2 ± 4.2
98/2	132.3 ± 5.0
85/15	130.0 ± 2.0

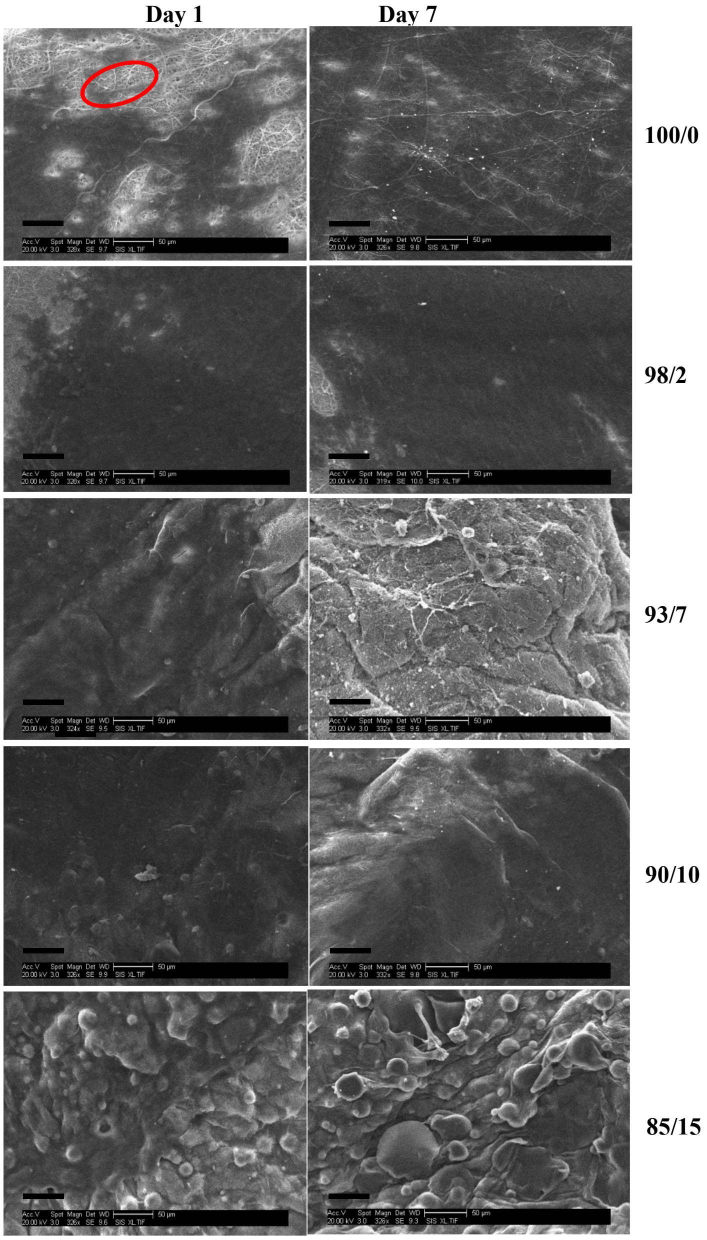

Figure 14: SEM images (scale bar = 50 µm) of cell seeded espun PCL/PMeDX scaffolds after days 1 and 7 respectively

Journal of Materials Chemistry B Accepted Manuscript

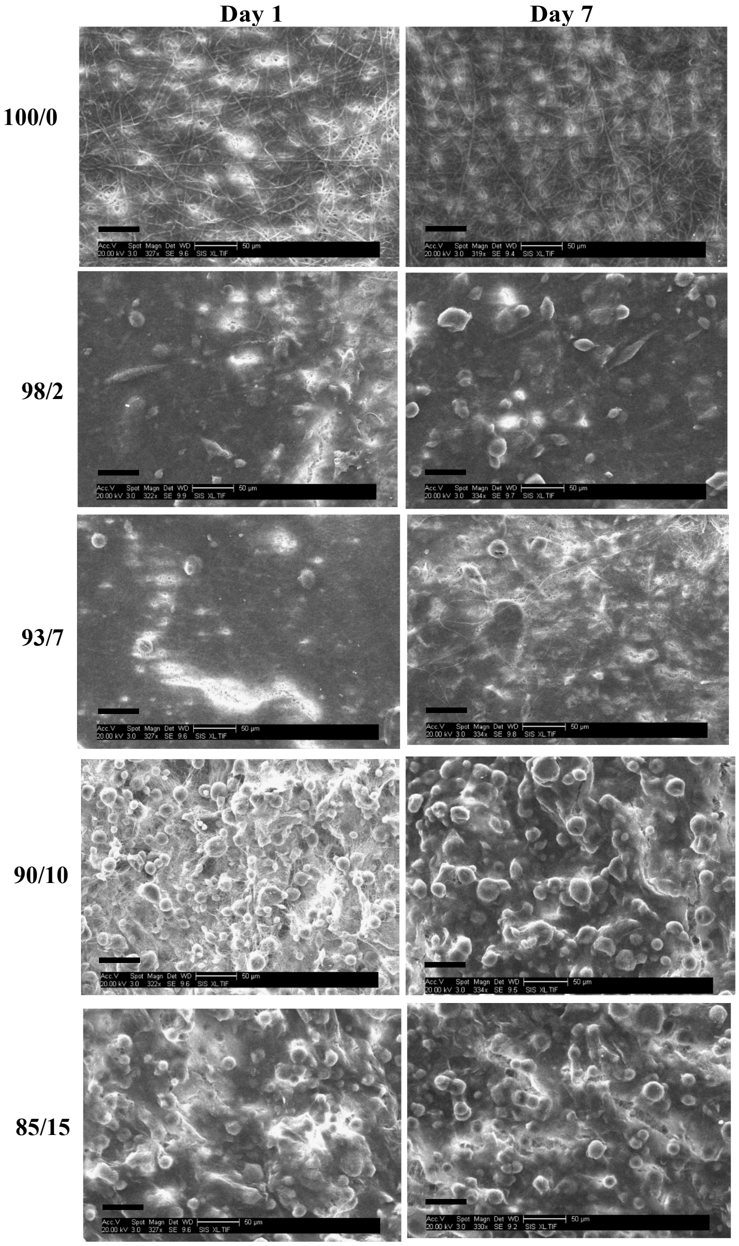

Figure 15: SEM of (scale bar = 50 µm) cell seeded espun PLLA/PMeDX scaffolds after days 1 and 7 respectively

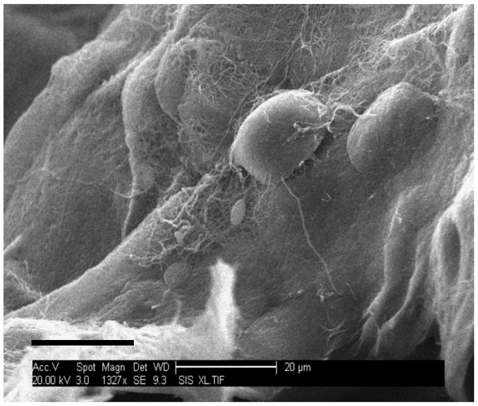

Figure 16: SEM of (1327× magnification, scale bar = 20 µm) cell seeded espun PCL/PMeDX 85/15 scaffolds after day 7

Cell infiltration

Engineered scaffolds should not only support cell attachment and proliferation but should also allow cell infiltration throughout the scaffolds so as to promote uniform tissue regeneration [69]. A major challenge therefore concerns the promotion of cellular ingrowth into espun scaffolds.

Cell-seeded espun PCL/PMeDX and PLLA/PMeDX mats were cryo-sectioned and stained with 4’-6-diamidino-2-phenylindole (DAPI) to image cell nuclei and determine cell migration. Figures 17 and 18 depict the fluorescence microscopy images of HDFs cultured on the scaffolds. HDFs appear as bright dots as can be noted from Figure 17. The depth of cellular infiltration was quantified and results summarised in Table 12. As detailed in the Experimental Section, we have privileged % migration rather than distance migration. As observed previously, espun PDX/PMeDX mats show an infiltration up to 45.1 % [45]. No infiltration is noted for PCL/PMeDX mats independently of PMeDX composition. Infiltration is observed in varying percentages for PLLA/PMeDX depending on composition. Noteworthy is the fact that a 85/15 blend shows a 100 % infiltration. Comparison of the different blend mats shows that cell morphology appears to be a dominating factor influencing cell infiltration. Indeed, in the case of PDX/PMeDX and PCL/PMeDX mats, HDFs adopt more of a spindle-shape whereas cells are more cobble-stone shaped in the case of espun PLLA/PMeDX mats. The pore size of the scaffold mat is also a determining factor. Indeed, literature reveals that HDFs start secreting ECM almost immediately in scaffolds with pore size less than 15 µm.

It is possible that the presence of corrugation-like structures in 85/15 PLLA/PMeDX scaffold enhanced cell infiltration. Indeed, as reported previously [70], microstructure and morphological features such as lamellar thickness or interlamellar distance were found to guide human mesenchymal stem cells (hMSCs) towards the interior of silk scaffold, producing a multilamellar hybrid construct [70].

Journal of Materials Chemistry B Accepted Manuscript

Table 12: Summary of HDF migration in espun PCL/PMeDX and PLLA/PMeDX mats

Blend composition (wt/wt %)	Depth of cellular migration (%)		
	Espun PDX/PMeDX	Espun PCL/PMeDX	Espun PLLA/PMeDX
100/0	0	0	0
98/2	45.1 ± 11.8		0
93/7	0		15.1 ± 5.68
90/10	0		4.65 ± 10.6
85/15	0		100

HDFs penetrated the full thickness of the 85/15 PLLA/PMeDX scaffold and were homogeneously distributed at day 7. All cells resided on the surface of the 85/15 PLLA/PMeDX scaffold at day 1. This suggests that cells observed within the scaffold at day 7 is a result of cell migration and not initial cell seeding. We can therefore conclude that espun 85/15 PLLA/PMeDX mat had the right combination of fibre diameter, pore size, porosity, mechanical and degradation properties. Such extensive cell migration is quite rare for espun materials without modification in porosity. Indeed, a number of methodologies have been proposed for improving cell infiltration. For instance, electrospinning has been combined with salt leaching to produce a PCL scaffold with engineered delaminations [71]. Up to 4 mm of cellular infiltration was observed after 3 weeks in culture. Another common method of increasing porosity of espun mats is via the selective removal of sacrificial fibres as reported in a study by Baker *et al.* [72]. Overall, cellular infiltration improved with increasing PEO content. At higher PEO contents, nearly complete infiltration was observed. However, some regions remained devoid of cells and cell distribution within the scaffold was non-homogeneous.

Overall cytocompatibility results indicate that the inclusion of PMeDX into espun PCL and PLLA scaffolds improves the *in vitro* bioactivity of the matrix through either chemical or mechanical signalling, or a combination of the two.

In summary, *in vitro* cell culture studies showed that compared to espun PCL and PLLA mats, a greater density of viable cells were observed on espun PCL/PMeDX and PLLA/PMeDX scaffolds respectively. Moreover, extensive HDF infiltration was noted in espun 85/15 PLLA/PMeDX mats.

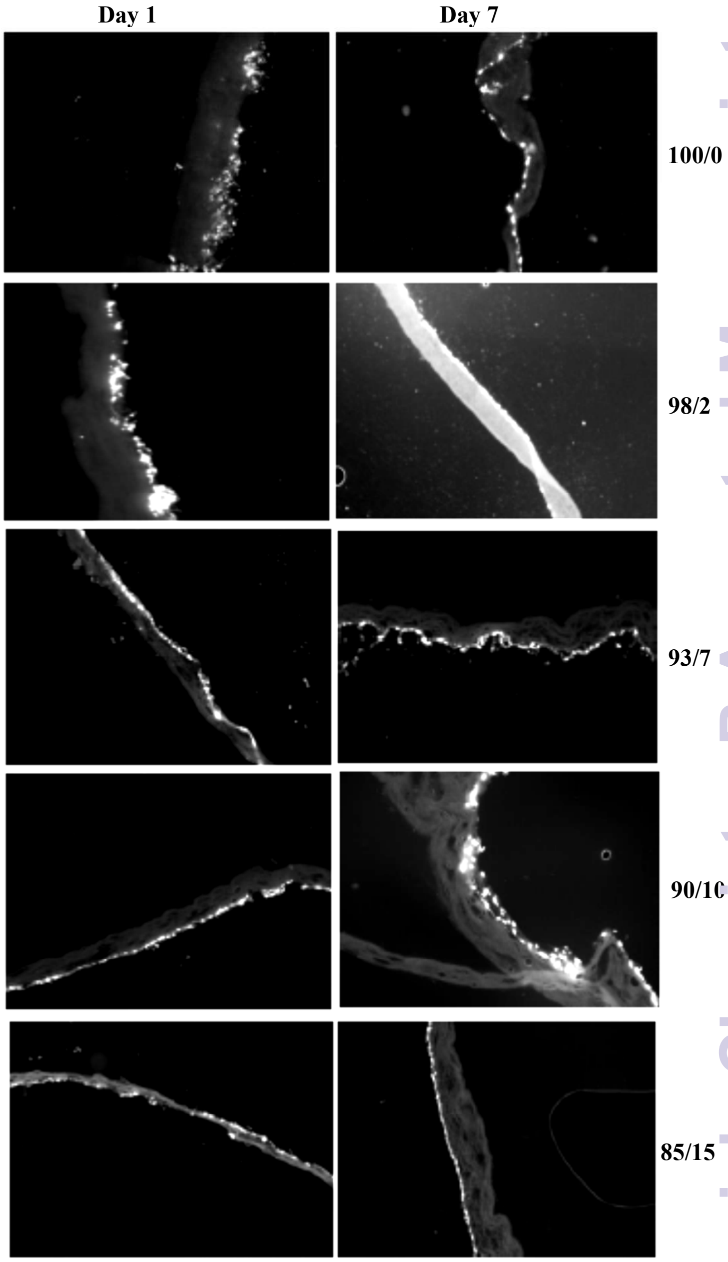

Figure 17: Fluorescence microscopy images (magnification 10×) of HDFs on espun PCL/PMeDX mats after days 1 and 7 respectively

Journal of Materials Chemistry B Accepted Manuscript

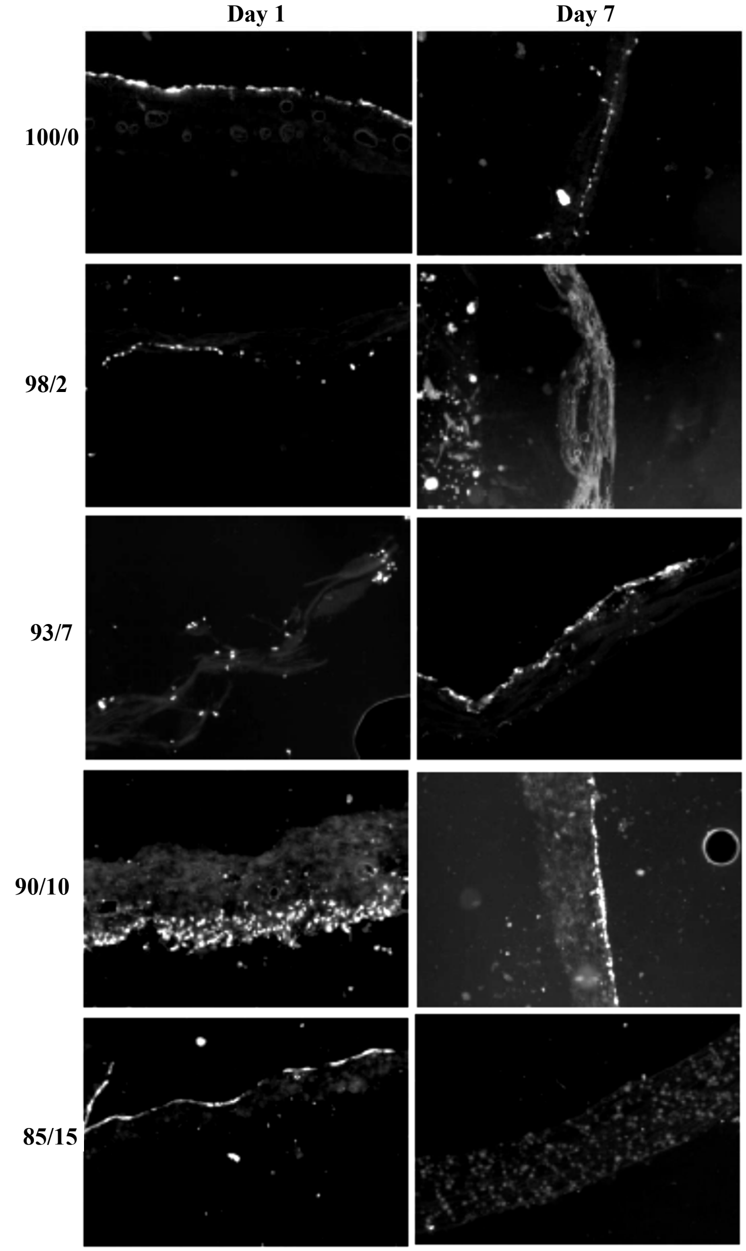

Figure 18: Fluorescence microscopy images (magnification 10×) of HDFs on espun PLLA/PMeDX mats after days 1 and 7 respectively

Experimental Section

Materials

Tin (II) octanoate (Alfa Aeser, 97 %) was used as received. Polycaprolactone (CAPA^{TM} 6500-inherent viscosity 2.45 at a concentration of 0.1 g/dL at 30 °C in 1,1,1,3,3,3 hexafluoroisopropanol) was obtained from Solvay Chemicals. Polylactic acid (Purasorb PL18, inherent viscosity of 1.8 at a concentration of 0.1 g/dL at 25 °C in chloroform) was purchased from Purac. D,L-3-methyl-1,4-dioxan-2-one was synthesized according to procedures previously described by us [73]. 1,1,1,3,3,3 hexafluoroisopropanol from Apollo Scientific Limited was used as received. Phosphate buffer solution (PBS) was purchased from Sigma-Aldrich and used as received.

Methods

Polymerization of 3-MeDX. A typical polymerization is hereby described. A solution of $Sn(Oct)_2$ was prepared by dissolving 0.1 g of $Sn(Oct)_2$ in toluene (5 ml) in a glove box. 29 μL of this solution was transferred to a quick fit tube containing 3-MeDX (1.16 g). The tube was then placed in a preheated oil bath at 80 °C. After the desired polymerization time, the reaction was quenched in liquid nitrogen and the crude sample purified by dissolving in chloroform and precipitating in petroleum ether. The product was then dried under vacuum before characterization by ^{1}H-NMR and ^{13}C-NMR.

Electrospinning of PCL/PMeDX and PLLA/PMeDX blends. PCL/PMeDX and PLLA/PMeDX were blended in the following ratios: 100/0, 98/2, 93/7, 90/10, and 85/15 wt/wt %. Each blend was immersed in HFIP in separate vials at a concentration of 100 mg/mL and left on a shaker plate overnight. The polymer solutions were then loaded into a 3 mL syringe and dispensed at a constant rate using a KD Scientific syringe pump. Electrospinning parameters were optimized (rate: 3.5 mL/hr, air-gap distance: 20 cm, voltage: +26 kV, grounded back target) to produce continuous, non-woven fibres which were collected on a rotating grounded rectangular mandrel (7.5 x 2.5 x 0.5 cm). After electrospinning, scaffolds were removed from the mandrel and stored in a desiccation chamber until further analysis.

Determination of porosity. The porosity of the scaffolds was measured using a method described by Soliman *et al.* [74]. Briefly, 10×10 mm^2 disks of the espun scaffolds were weighed and subsequently immersed in 70% ethanol overnight with slight mechanical agitation. This was done to allow the ethanol to penetrate into the scaffold pores. The surface of the samples was then blotted dry on a filter paper and weighed once more to determine the mass of the ethanol present within the scaffold. Measurements were made on three samples of each scaffold type. The density of ethanol, PCL and PLLA are 0.788, 1.123 and 1.23 g/ml respectively. The porosity (ε) was calculated as:

$$\varepsilon = \frac{V_{EtOH}}{V_{EtOH}+V_{PCL}} \qquad (1)$$

where V_{EtOH} is the volume of the intruded ethanol and was calculated as the ratio of the observed mass change after intrusion and ρ_{EtOH}. V_{PCL} is the volume of PCL fibres and was calculated as the ratio between the dry scaffold mass before intrusion and the density of PCL (ρ_{PCL}).

Non-isothermal crystallization kinetics. Non-isothermal crystallization kinetics was investigated using Equations 2 and 3 as detailed in our recent paper [45].

$$X_t(T) = \frac{\int_{T_0}^{T}\left(\frac{dH_c}{dT}\right) \times dT}{\Delta H_c} \qquad (2)$$

T_0: onset temperature of crystallization
T: an arbitrary temperature
dH_c/dT: variation of the enthalpy of crystallization as a function of temperature variation
ΔH_c: total enthalpy of crystallization at a specific cooling rate

$$t = \frac{T_0 - T}{\beta} \qquad (3)$$

t: time
T: temperature
β: constant cooling rate.

Journal of Materials Chemistry B Accepted Manuscript

Hydrolytic degradation of electrospun mats. Espun mats were placed in PBS at 37 ^{0}C for five weeks. After each degradation period, the samples were washed and dried under vacuum. % mass loss and % weight retention were calculated according to equations 4 and 5 respectively.

$$\%\ \text{mass loss} = \frac{Initial\ mass/g - Final\ mass/g}{Initial\ mass/g} \times 100 \qquad (4)$$

$$\%\ \text{weight retention} \frac{Final\ mass/g}{Initial\ mass/g} \times\ 100 \qquad (5)$$

***In vitro* biocompatibility studies.** Cell culture and migration studies were carried out using human dermal fibroblasts. The experimental protocol was similar to the one used in our previous paper [45]. To standardize the variation in scaffold thickness, cell migration was analysed as a percentage of distance travelled with respect to the thickness at that spot instead of solely distance travelled. % migration (n=30) was calculated according to Equation 5.

$$\%\ \text{migration} = \frac{\text{distance of cell migration from the top}}{\text{thickness of scaffold at that exact point}} \times 100 \qquad (5)$$

Measurements

Differential Scanning Calorimetry (DSC) analysis was carried out using a Netzsch DSC 200 F3 Maia® thermal analyzer (Chennai, India). All PCL/PMeDX blend samples were heated from 30 to 80 °C, cooled to -30 °C and reheated to 80 °C at 3 °C/min. All PLLA/PMeDX blend samples were heated from 30 to 180 °C, cooled to -30 °C and reheated to 180 °C at 3 °C/min. Netzsch TG 209 F3 Tarsus® analyzer (Chennai, India) was used to measure and record the sample mass change with temperature over the course of the pyrolysis reaction. Thermogravimetric curves were obtained at a heating rate of 10 °C/min between 25 °C and 700 °C. Nitrogen was used as an inert purge gas to displace air in the pyrolysis zone, thus avoiding unwanted oxidation of the sample. The sample mass used in this study was approximately 10 mg. SEM data were acquired on a Philips XL 30 scanning electron microscope operated at an acceleration voltage of 20 kV using the secondary electron detector. The polymer samples were sputter-coated with gold (5 nm thick) before imaging (Edwards, UK). Inner (in contact with mandrel) surface of the espun mats were imaged. To determine fibre and pore size, the ImageTool 3.0 image analysis software package was used (Shareware provided by University of Texas Health Science Center at San Antonio). The software was calibrated using the micron scale bar of each picture. An average fibre diameter was determined by measuring the diameter of 60 different fibres, while an average pore size was determined by measuring the diameter of 60 different pores. Pores were identified as areas of void space bounded by fibres on all sides at or near the same depth of field, while their long and short diagonal axes were measured and averaged together to serve as their diameter [75]. Intermittent contact (tapping) mode AFM imaging was done on as prepared samples on an Asylum MFP-3D atomic force microscope (Asylum Research, USA) using Olympus AC160TS cantilevers (with a resonance frequency of 300 kHz and a nominal spring constant of 40 N/m) under ambient conditions. The rms amplitude of the cantilever was adjusted to 85 nm and a setpoint ratio of 0.8 was chosen. Constant amplitude images were acquired, depending on the scan size, with 512 pixels x 512 pixels (up to 2024 pixels x 2024 pixels); the phase shift was recorded simultaneously. The data was processed off line using the MFP-3D software. Tensile properties of the espun mats (40 x 10 x 4 mm^3) were studied utilizing an Instron Tensile Tester 3343 (Instron, USA) at 27 °C and 60 % relative humidity using a crosshead speed of 10 mm/min, gauge length of 1 cm and 500 N load cell. Errors in Young`s modulus and strain were calculated as reported in our previous paper [45]. The contact angles of the modified surfaces were measured using water as a probe liquid (Milli-Q water from a Millipore Direct-Q 8 system with resistivity of 18.0MΩ/cm) with an OCA 15plus instrument (Data Physics Instruments GmbH, Germany). Static contact angle data based on the sessile drop method were acquired immediately after deposition of a 1 μL drop on at least three positions for each sample and are stated as arithmetic mean. A short film sequence covering several seconds before and after deposition of the droplet was taken.

Conclusions

Espun PCL/PMeDX and PLLA/PMeDX mats were successfully fabricated from HFIP solutions. FTIR and TGA analysis showed that immiscibility increases with increasing PMeDX content for espun PCL/PMeDX fibres, with the 98/2 blend being partially miscible. AFM images revealed that espun PCL/PMeDX mats showed a rougher surface compared to espun PCL mat, possibly due to dispersion of PMeDX within the PCL matrix. Addition of PMeDX caused a change in the width of the lamellae as was noted from AFM images. Espun PLLA/PMeDX fibres exhibit corrugation-like patterns. The drop in mechanical properties of espun PCL/PMeDX was explained by the likely formation of phase boundaries which impact on mechanical performance more than crystallinity changes. No clear trend was observed with increasing PMeDX content for espun PLLA/PMeDX due possibly to antagonist effects such as drop in crystallinity which impacts negatively on mechanical properties (98/2 composition) and formation of stereocomplex. Degradation of espun mats occurred via a surface erosion mechanism. In addition, biocompatibility studies conducted using HDFs showed that in general, espun PCL/PMeDX and PLLA/PMeDX scaffolds supported cell growth better than the corresponding espun homopolymer mats. Correlation of physico-chemical properties with biological performance is very complex and the nature of the polymer plays a key role. Adjustment of physico-chemical and mechanical properties to match bio-performance requires careful investigation almost on a case by case basis.

Acknowledgements

We thank the Tertiary Education Commission (Mauritius) for awarding a PhD scholarship to N. Goonoo. We are grateful to the Mauritius Research Council (Mauritius) for supporting biomaterials and drug delivery research at the ANDI Centre of Excellence for Biomedical and Biomaterials Research (CBBR). We acknowledge the input from Gary Bowlin's group at University of Memphis for assistance with electrospinning and cell culture studies. Daniel Wesner and Holger Schönherr acknowledge financial support from the Deutsche Forschungsgemeinschaft (DFG instrument grant no. INST 221/87-1FUGG) and the European Research Council (ERC starting grant to HS, ERC grant agreement no. 279202).

Notes and References

[a]ANDI Centre of Excellence for Biomedical and Biomaterials Research, MSIRI Building, University of Mauritius, Réduit, Mauritius;
[b]Biomedical Engineering Department, University of Memphis, 330 Engineering Technology, Memphis, USA;
[c]Physical Chemistry I, Department of Chemistry and Biology, University of Siegen, 57076 Siegen, Germany
[*] Corresponding author; E-mail: djhurry@uom.ac.mu

Journal of Materials Chemistry B Accepted Manuscript

1. J. M. Holzwarth and P. X. Ma, *Journal of Materials Chemistry,* 2011, **21**, 10243-10251.
2. M. N. Collins and C. Birkinshaw, *Carbohydrate Polymers*, 2013, **92**, 1262–1279.
3. N. Goonoo, A. Bhaw-Luximon, G. L. Bowlin and D. Jhurry, *Polymer International,* 2013, **62(4)**, 523–533.
4. L. S. Nair and C. T. Laurencin, *Advances in Biochemical Engineering/ Biotechnology,* 2006, **102**, 47–90.
5. Q. Cai, Y. Wan, J. Bei and S. Wang, *Biomaterials,* 2003, **24**, 3555-3562.
6. Q. Cai, J. Yang and S. Wang, *Biomaterials*, 2002, **23**, 4483-4492.
7. J. Venugopal, L. L. Ma, T. Yong and S. Ramakrishna, *Cell Biology International*, 2005, **29**, 861–867.
8. J. R. Venugopal, Y. Zhang and S. Ramakrishna, *Artificial Organs,* 2006, **30(6)**, 440–446.
9. S. Srouji, T. Kizhner, E. Suss-Tobi, E. Livne and E. Zussman, *Journal of Materials Science: Materials in Medicine,* 2008, **19**, 1249–1255.
10. J. S. Choi, S. J. Lee, G. J. Christ, A. Atala, J. J. Yoo, *Biomaterials,* 2008, **29(19)**, 2899–2906.
11. X. Yang, J. D. Shah and H. Wang, *Tissue Engineering A*, 2009, **15(4)**, 945–956.
12. Y. M. Ju, J. S. Choi, A. Atala, J. J. Yoo, S. J. Lee, *Biomaterials*, 2010, **31(15)**, 4313–4321.
13. Y. Zhang, H. Ouyang, C. T. Lim, S. Ramakrishna and Z. M. Huang, *Journal of Biomedical Materials Research,* 2005, **72(1)**, 156–165.
14. Z. Ma, W. He, T. Yong and S. Ramakrishna, *Tissue Engineering*, 2005, **11(7/8)**, 1149–1158.
15. E. J. Chong, T. T. Phan, I. J. Lim, Y. Z. Zhang, B. H. Bay, S. Ramakrishna and C. T. Lim, *Acta Biomaterialia,* 2007, **3**, 321–330.
16. R. S. Tigli, N. M. Kazaroğlu, I. S. B. Mav and I. O. M. Gümüşderel, *Journal of Biomaterials. Science, Polymer Edition*, 2011, **22(1–3)**, 207–223.
17. S. Gautam, A. K. Dinda and N. C. Mishra, *Materials Science and Engineering C,* 2013, **33**, 1228–1235.
18. Y. C. Lim, J. Johnson, Z. Fei, Y. Wu, D. F. Farson, J. J. Lannutti, H. W. Choi and L. J. Lee, *Biotechnology and Bioengineering*, 2011, **108(1)**, 116–126.
19. S. J. Lee, J. Liu, S. H. Oh, S. Soker, A. Atala, and J. J. Yoo, *Biomaterials*, 2008, **29**, 2891-2898.
20. Y. Zhang, H. Ouyang, C. T. Lim, S. Ramakrishna and Z. M. Huang, *Journal of Biomedical Materials Reseach Part B*, 2005, **72 B(1)**, 156-165.
21. R. Mehdinavaz Aghdam, S. Najarian, S. Shakhesi, S. Khanlari, K. Shabaani and S. Sharifi, *Journal of Applied Polymer Science*, 2012, **124(1)**, 123–131.
22. J. H. Kim, P. H. Choung, I. Y. Kim, K. T. Lim, H. M. Son, Y. H. Choung, C. S. Cho and J. H. Chung, *Materials Science and Engineering C*, 2009, **29**, 1725-1731.
23. J. Han, C. J. Branford-White and L. M. Zhu, *Carbohydrate Polymers*, 2010, **79**, 214-218.
24. S. R. Son, N. T. Ba-Linh, H. M. Yang and B. T. Lee, *Science and Technology of Advanced Materials,* 2013, **14(1)**, 015009.
25. S. Y. Gu, Z. M. Wang, J. Ren and C. Y. Zhang, *Materials Science and Engineering C*, 2009, **29**, 1822–1828.
26. P. Torricelli, M. Gioffre, A. Fiorani, S. Panzavolta, C. Gualandi, M. Fini, M. L. Focarete and A. Bigi, *Materials Science and Engineering C*, 2014, **36**, 130–138.
27. S. Wang, Y. Zhang, H. Wang, g. Yin and Z. Dong, *Biomacromolecules,* 2009, **10(8)**, 2240-2244.
28. K. T. Shalumon, D. Sathish, S. V. Nair, K. P. Chennazhi, H. Tamura and R. Jayakumar, *Journal of Biomedical Nanotechnology*, 2012, **8(3)**, 405-416.
29. H. Liu and S. D. Wang, *Journal of Textile Research,* 2012, **33(2)**, 21-25.
30. L. Chen, Y. Bai, G. Liao, E. Peng, B. Wu, Y. Wang, X. Zeng and X. Xie, *PLoS One*, 2013, **8(8)**, 71265.
31. A. C. Areias, C. Ribeiro, V. Sencadas, N. Garcia-Giralt, A. Diez-Perez, J. L. Gomez-Ribelles and S. Lanceros-Mendez, *Soft Matter*, 2012, **8**, 5818-5825.
32. B. B. Mandal and S. C. Kundu, *Biomaterials,* 2009, **30**, 2956-2965.
33. P. C. George, W. J. Miller, D. F. Meany, E. S. Sawyer and P. A. Janmey, *Biophysical Journal,* 2006, **90**, 3012-3018.
34. G. Ladam, L. Vonna, and Sackmann E, *Acta Biomaterialia*, 2005, **1**, 485-497.
35. J. Solon, I. Levental, K. Sengupta, P. C. Georges and P. A. Janmey, *Biophysical Journal,* 2007, **93**, 4453–4461.
36. R. J. Pelham and Y. L. Wang, *Proceedings of the National Academy of Sciences USA*, 1997, **94**, 13661-5.
37. T. Yeung, P. C. Georges, L. A. Flanagan, B. Marg, M. Ortiz et al. *Cell Motility and the Cytoskeleton*, 2005, **60**, 24-34.
38. H. Cui and P. J. Sinko, *Frontiers of Materials Science*, 2012, **6(1)**, 47-59.
39. A. K. Yip, K. Iwasaki, C. Ursekar, H. Machiyama, M. Saxena, H. Chen, I. Harada, K. H. Chianm and Y. Sawada, *Biophysical Journal*, 2013, **104(1)**, 19-29.
40. C. M. Lo, H. B. Wang, M. Dembo and Y. L. Wang *Biophysical Journal*, 2000, **79**, 144 –152.
41. J. Yang, Y. Wan, C. Tu, Q. Cai, J. Bei and S. Wang, *Polymer International,* 2003, **52**, 1892-1899.
42. A. Hezi-Yamit, C. Sullivan, J. Wong, L. David, M. Chen, P. Cheng, et al., *Journal of Biomedical Materials Research Part A*, 2009, **90(1)**, 133-141.
43. Y. Arima and H. Iwata, *Biomaterials*, 2007, **28**, 3074-3082.
44. N. Goonoo, A. Bhaw-Luximon, I. A. Rodriguez, G. L. Bowlin and D. Jhurry, *International Journal of Polymeric Materials and Polymeric Biomaterials,* 2014, **63(10)**, 1–11.
45. N. Goonoo, A. Bhaw-Luximon, I. A. Rodriguez, D. Wesner, H. Schönherr, G. L. Bowlin and D. Jhurry, *Biomaterials Science,* 2014, **2(3)**, 339–351.
46. V. Crescenzi, G. Manzini, G. Calzolari and C. Borri, *European Polymer Journal* 1972, **8(3)**, 449-463.
47. E. W. Fisher, H. J. Sterzel and G. Wegner, *Kolloid-ZZ Polimere* 1973, **251**, 980-990.
48. A. A. C. M. Oudhuis, H. J. Thiewes, P. F. Van Huten, G. Ten Brinke, *Polymer*, 1994, **35(18)**, 3936-3942.
49. Y. Liu, J. Shao, J. Sun, X. Bian, L. Feng, S. Xiang, B. Sun, Z. Chen, G. Li, X. Chen, *Polymer Degradation and Stability*, 2014, **101**, 10-17.

Journal of Materials Chemistry B Accepted Manuscript

50. T. Okihara, M. Tsuji, A. Kawaguchi, K. Katayama, H.Tsuji, S.-H. Hyon, Y. Ikada, *J. Macromol. Sci., Phys.*, 1991, **B30**, 119.
51. W. Hoogsteen, A. R. Postema, A. J. Pennings, G. Tenbrinke, P. Zugenmaier, *Macromolecules,* 1990, **23**, 634-642.
52. J. Slager, A. J. Domb, *Biomacromolecules,* 2003, **4**, 1308-1315.
53. A. Leclair, B. D. Favis, *Polymer*, 1996, **37(21)**, 4723-2728.
54. E. Y. Gomez-Pachon, R. Vera- Graziano, R. Montiel Campos, *IOP Conf. Ser.: Mater. Sci. Eng.* **59**, 012003 doi:10.1088/1757-899X/59/1/012003.
55. J. H. Han, C. Choi-Feng, D. J. Li and C. Dae-Han, *Polymer*, 1995, **36**, 2451-2462.
56. D. H. Reneker, A. L. Yarin, H. Fong and S. Koombhonghse, *Journal of Applied Physics*, 2000, **87(9)**, 4531-4547.
57. A. Baji, Y. W. Mai, S. C. Wong, M. Abtahi and P. Chen, *Composites Science and Technology*, 2010, **70(5)**, 703-718.
58. X. Wei, Z. Xia, S. C. Wong and A. Baji, *International Journal of Experimental and Computational Biomechanics*, 2009, **1(1)**, 45-57.
59. S. C. Wong, A. Baji and S. W. Leng, *Polymer,* 2008, **21**, 4713–4722.
60. A. Camposeo, I. Greenfeld, F. Tantussi, S. Pagliara, M. Moffa, F. Fuso, M. Allegrini, E. Zussman and D. Pisignano, *Nano Letters*, 2013, **13**, 5056−5062.
61. S. Mishra, A. Viano, N. Fore, G. Lewis, A. Ray, *Bio-Medical Materials and Engineering*, 2003, **13(2)**, 135-146.
62. A. Saffar, A. Ajji, P. J. Carreau, M. R. Kamal, *Polymer*, 2014, **55**, 3156-3167.
63. D. Bozic, I. C. M. Vilotijevic, M. T. Jovanovic, *J. Serb. Chem. Soc.* 2006, **71 (8–9)**, 985–992.
64. C. C. Chen, J. Y. Chueh, H. Tseng, H. M. Huang, S. Y. Lee, Biomaterials 2003, **24**, 1167–1173.
65. M. L. Zhao, G. Sui, X. L. Deng, J. G. Lu, S. K. Ryu and X. P. Yang, *Advanced Materials Research,* 2006, **11-12**, 243-246.
66. L. G. Braddon, D. Karoyli, D. G. Harrison, and R. M. Nerem, *Tissue Engineering*, 2002, **8(4)**, 695-708.
67. D. Ajami-Henriquez, M. Rodríguez, M. Sabino, R. V. Castillo, A. J. Müller, A. Boschetti-de-Fierro, C. Abetz, V. Abetz, P. Dubois, *Journal of Biomedical Materials Research Part A*, 2008, **87A(2)**, 405–417.
68. A. K. Salem, R. Stevens, R. G. Pearson, M. C. Davies, S. J. B. Tendler, C. J. Roberts, P. M. Williams and K. M. Shakesheff, *Journal of Biomedical Materials Research,* 2002, **61(2)**, 212-217.
69. B. A. Blackeney, A. Tambralli, J. M. Anderson, A. Andukuri, D. J. Lim, D. R. Dean and H. W. Jun, *Biomaterials*, 2011, **32**, 1583-1590.
70. A.L. Oliveira, L. Sun, H. J. Kim, X. Hu, W. Rice, J. Kluge, R. L. Reis, D. L. Kaplan, *Acta Biomaterialia*, **2012**, 8(4), 1530–1542.
71. J. Nam, Y. Huang, S. Agarwal, J. Lannutti, *Tissue Engineering,* 2007, **13(9),** 2249-2257
72. B. M. Baker, A. O. Gee, R. B. Metter, A. S. Nathan, R. A. Marklein, J. A. Burdick, R. L. Mauck, *Biomaterials,* 2008, **29(15)**, 2348–2358.
73. Y. Lochee, D. Jhurry, A. Bhaw-Luximon and A. Kalangos, *Polymer International,* 2010, **59**, 1310–1318.
74. S. Soliman, S. Sant, J. W. Nichol, M. Khabiry, E. Traversa and A. Khademhosseini, *Journal of Biomedical Materials Research A*, 2011, **96(3)**, 566-574
75. S. Sell, C. Barnes, D. Simpson and G. Bowlin, *Journal of Biomedical Materials Research A*, 2008, **85**, 115-126

Journal of Materials Chemistry B Accepted Manuscript

This journal is © The Royal Society of Chemistry 2012

Graphical Abstract

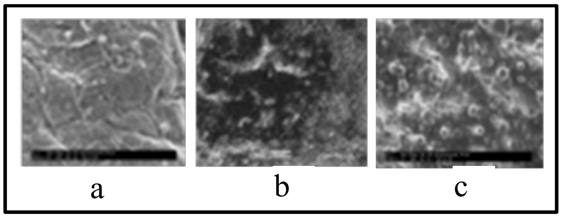

SEM images of HDF cells on scaffolds: (a) PCL/PMeDX: 93/7- good adhesion and proliferation, (b) PDX/PMeDX: 98/2- good adhesion, proliferation & infiltration and (c) PLLA/PMeDX: 85/15- good proliferation and infiltration

Journal of Materials Chemistry B Accepted Manuscript